Brain Stimulation 12 (2019) 1500–1507

Contents lists available at ScienceDirect

Brain Stimulation

journal homepage: http://www.journals.elsevier.com/brain-stimulation

Real-time estimation of electric fields induced by transcranial magnetic stimulation with deep neural networks

Tatsuya Yokota [a, c, *], Toyohiro Maki [a], Tatsuya Nagata [a], Takenobu Murakami [d], Yoshikazu Ugawa [e], Ilkka Laakso [f], Akimasa Hirata [b, c], Hidekata Hontani [a, c]

[a] Department of Computer Science, Nagoya Institute of Technology, Aichi, Japan
[b] Department of Electrical and Mechanical Engineering, Nagoya Institute of Technology, Aichi, Japan
[c] Center of Biomedical Physics and Information Technology, Nagoya Institute of Technology, Aichi, Japan
[d] Department of Neurology, Fukushima Medical University, Fukushima, Japan
[e] Department of Neuro-Regeneration, Fukushima Medical University, Fukushima, Japan
[f] Department of Electrical Engineering and Automation, Aalto University, Espoo, Finland

ARTICLE INFO

Article history:
Received 4 January 2019
Received in revised form
11 June 2019
Accepted 12 June 2019
Available online 17 June 2019

Keywords:
Deep neural networks
Transcranial magnetic stimulation
Magnetic resonance image
Electric field estimation
Volume conductor modeling

ABSTRACT

Background: Transcranial magnetic stimulation (TMS) plays an important role in treatment of mental and neurological illnesses, and neurosurgery. However, it is difficult to target specific brain regions accurately because the complex anatomy of the brain substantially affects the shape and strength of the electric fields induced by the TMS coil. A volume conductor model can be used for determining the accurate electric fields; however, the construction of subject-specific anatomical head structures is time-consuming.

Objective: The aim of this study is to propose a method to estimate electric fields induced by TMS from only T1 magnetic resonance (MR) images, without constructing a subject-specific anatomical model.

Methods: Very large sets of electric fields in the brain of subject-specific anatomical models, which are constructed from T1 and T2 MR images, are computed by a volume conductor model. The relation between electric field distribution and T1 MR images is used for machine learning. Deep neural network (DNN) models are applied for the first time to electric field estimation.

Results: By determining the relationships between the T1 MR images and electric fields by DNN models, the process of electric field estimation is markedly accelerated (to 0.03 s) due to the absence of a requirement for anatomical head structure reconstruction and volume conductor computation. Validation shows promising estimation accuracy, and rapid computations of the DNN model are apt for practical applications.

Conclusion: The study showed that the DNN model can estimate the electric fields from only T1 MR images and requires low computation time, suggesting the possibility of using machine learning for real-time electric field estimation in navigated TMS.

Introduction

Transcranial magnetic stimulation (TMS) is a technique for stimulating a target area of the brain in a non-invasive manner. Impulsive and intense current injected into a stimulation coil located just above the scalp induces a focal electric field (E-field) in the brain. Single- or multiple (repetitive)-pulse TMS is often used for diagnosis in pre-surgical identification of motor and language functions, as well as for therapy, such as that for neuropathic pain and enhancing motor recovery [1]. Bottlenecks in TMS-based diagnosis include its reliability being dependent on the experience of the operators, the time needed for the diagnosis, as well as the choice of optimal stimulation parameters.

The stimulation strength of TMS has been thought to be maximal just below the coil center, where the coil current is at its maximum. However, recent experimental and computational studies suggested that the maximal stimulation strength does not

* Corresponding author. Department of Computer Science, Nagoya Institute of Technology, Aichi, Japan.
E-mail addresses: t.yokota@nitech.ac.jp (T. Yokota), hontani@nitech.ac.jp (H. Hontani).

https://doi.org/10.1016/j.brs.2019.06.015

always occur at this estimated location [2]. The reason for this discrepancy is attributable to the complex structure of human brain anatomy, as predicted by recent computational studies [3–8].

Recently, computational studies have been conducted to estimate the E-field in certain subjects by using volume conductor models based on subject-specific human head models. The E-field is known as the main physical agent, and notably, its relative direction to neural structures is also important. From a practical viewpoint, it is used as a surrogate for stimulation volume. The effectiveness of such modeling has been confirmed by comparing computationally estimated volumes with those identified by direct electric stimulation measured in neurosurgery studies [9,10]. This computational approach is helpful for planning diagnoses and therapy.

A concern associated with this approach is that the computational cost is generally substantial, including the cost associated with the development of a subject-specific human head model and computation using a volume conductor model. The latter takes tens of seconds to a few minutes to estimate the E-field in the brain for one location and angle of the TMS coil, and it is dependent on factors such as the model resolution and computational resources. This issue has been mostly resolved by accelerating the algorithm of volume conductor modeling; our in-house software based on a geometric multi-grid reduces this time to several seconds or less [11]. Fast multi-pole methods have also been used to accelerate boundary element techniques [12]. However, the computation times are still too long for real-time calculations. Another important bottleneck is that it still takes few hours to half a day to develop a patient-specific human head model. Specifically, the process of segmenting the magnetic resonance (MR) image into brain tissues is time-consuming; FreeSurfer [13–15] or BrainVoyager[1] are often used for this purpose, and other software packages are used for the remaining tissues. These software packages have been integrated into segmentation pipelines such as SimNIBS [6], which can automatically generate segmented volume conductor models from T1 and T2 MR images. However, the quality of the segmentation is somewhat dependent on the MR image quality, and the developed models always need to be verified manually.

This study is the first proposal for real-time estimation of E-fields induced by TMS with "deep learning" [16], which directly regresses E-fields from only T1 MR without using the time-consuming segmentation software (*e.g.*, FreeSufer). This is a data-driven approach for E-field estimation: the mapping from only T1 MR images to E-fields is performed using training data consisting of a large number of pairs of T1 MR images and the corresponding E-fields. The mapping is represented by parametric models based on deep convolutional neural networks, which are hierarchically structured with convolution, max-pooling, and up-sampling layers. We employed a network architecture called "U-Net" [17], which is a fully convolutional network with multi-scale skip connections, for our regression task, and it is trained using more than 200,000 segments of MR and E-field pairs for generalizing various parts of the brain and TMS coil positions. After training and optimizing the deep neural network (DNN), the E-fields induced by the TMS coil can be directly estimated from only T1 MR images. In other words, the proposed machine learning approach can be immediately applied to new subjects after scanning the T1 MR images without the time-consuming process of constructing the subject-specific anatomical head model. Another advantage of this approach is that the computation time is only 0.01–0.03 s with a graphics processing unit (GPU), which is markedly reduced from the conventional approach (i.e., a few hours for anatomical segmentation as well as at least several seconds for computation), and allows calculations to be performed in real time during navigated TMS.

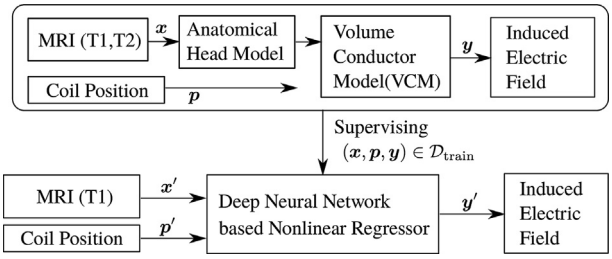

Fig. 1. Methodological design: A machine learning approach for estimating the E-field. The conventional physical model-based method constructs a subject-specific anatomical head model and estimates the E-field using a volume conductor model based on the conductivities of individual brain tissues. By exploiting the number of inputs and outputs generated by the physical model as a supervisor, the DNN model automatically *learns* the relationship between patterns of MR images and the corresponding E-fields. After learning from sufficient data, the appropriate E-fields can be estimated from new MR patterns.

Materials and methods

Methodological design

Mathematically, the objective of this study is to estimate an E-field $\boldsymbol{y}$ induced by TMS from a brain MR image $\boldsymbol{x}$ and a coil position $\boldsymbol{p}$. The proposed method is designed based on nonlinear regression problem inputting $(\boldsymbol{x}, \boldsymbol{p})$ and outputting $\boldsymbol{y}$. Fig. 1 shows the overall design of the proposed method. The method is separated into two phases: a training phase and an application phase. In the training phase, a physical model-based computation method [11] generates the training data $(\boldsymbol{x}, \boldsymbol{p}, \boldsymbol{y})$ as a supervisor in machine learning. Then, the DNN model is optimized for fitting the training data $(\boldsymbol{x}, \boldsymbol{p}, \boldsymbol{y})$ so that it imitates the supervisor. After the training using a large number of samples $(\boldsymbol{x}, \boldsymbol{p}, \boldsymbol{y}) \in \mathscr{D}_{\text{train}}$ is complete, the constructed regressor can be applied to a new MR image $\boldsymbol{x}'$ with any coil positions $\boldsymbol{p}'$ for estimating its induced E-field $\boldsymbol{y}'$.

Data, computation, and learning

We used the MR images of $N_x := 37$ subjects (Male 30, Female 7, Age 18–55), obtained at Fukushima Medical University and database.[2] All images were acquired using T1-and T2-weighted sequences with two different 3-T MR scanners: Siemens 3 T with MPRAGE sequence and GE 3 T with fast SPGR sequence. Each MR image was segmented with FreeSurfer into gray matter, white matter, cerebellum, brainstem, and various nuclei. Furthermore, non-brain tissue compartments were segmented with the 2D-histogram of the T1 and T2 images into blood, dura, cerebrospinal fluid, compact bone, spongy bone, fat, muscle, and skin. Fig. 2 shows the process for constructing the volume conductor model (VCM) from T1-and T2-weighted MR images. Thereafter, the VCMs were constructed for all MR images, and the induced E-fields, $\boldsymbol{y}$, with any combination of MR images and TMS coil positions, $(\boldsymbol{x}, \boldsymbol{p})$, could be calculated using the finite element method [11] using a figure-of-8 magnetic coil model that was constructed based on previous E-field measurements of the Magstim 70 mm Double Coil (The Magstim Company Ltd., UK) [19]. Details for constructing the VCMs and the electric field calculations are provided in the Supplementary Material.

[1] http://www.brainvoyager.com/.

[2] NAMIC: Brain Multimodality http://hdl.handle.net/1926/1687.

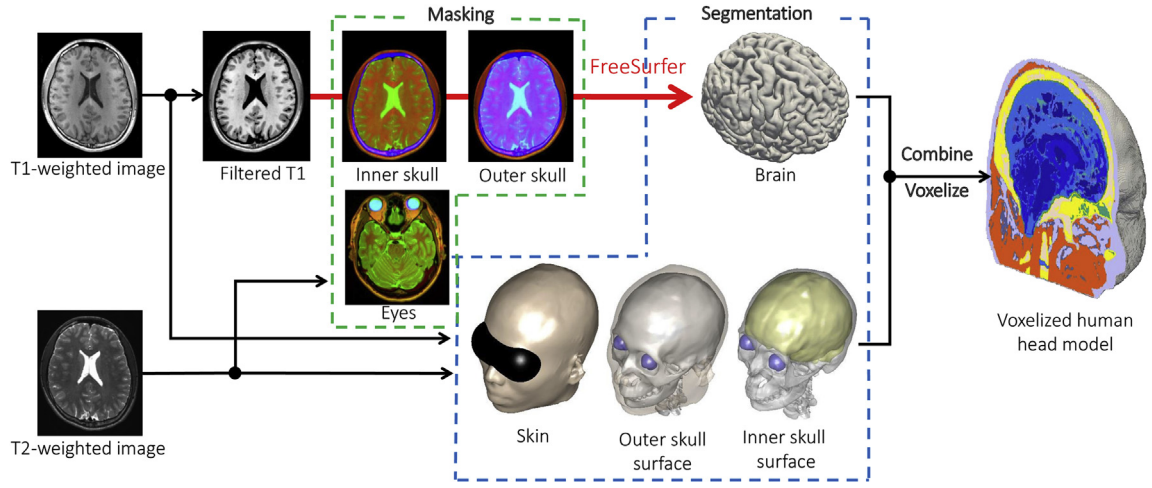

Fig. 2. MR images and segmented anatomical model: The anatomical head model is constructed from T1-and T2-weighted MR images. Brain tissues are segmented into gray matter, white matter, cerebellum, brain stem, and various nuclei by using FreeSurfer, and non-brain tissues are segmented into blood, dura, cerebrospinal fluid, compact bone, spongy bone, fat, muscle, and skin based on a two-dimensional histogram of T1-and T2-weighted MR image intensities.

For each subject, we computed E-fields for various TMS coil positions: total $N_p = 7056$ positions combining (14×14) locations and 36 angles. Fig. 3 shows examples of (14×14) TMS coil locations and angles. The TMS coil is located in a reticular pattern around the motor cortex. At each point, the TMS coil is rotated around the normal line of the brain surface at 10-degree intervals: $\{0^\circ, 10^\circ, 20^\circ, \ldots, 350^\circ\}$. Finally, we obtained a total of $N := N_x N_p = 261{,}072$ pairs of MR images and TMS coil positions, $\{\boldsymbol{x}_n, \boldsymbol{p}_n\}_{n=1}^N$, and their corresponding E-fields, $\{\boldsymbol{y}_n\}_{n=1}^N$.

We considered a parametric nonlinear regression model $r(\boldsymbol{x}, \boldsymbol{p}|\Theta)$, where Θ is a set of model parameters. Let $\mathscr{T}_{\text{train}} \subset \mathscr{D}$ be a set of training samples. We optimized Θ using the following criterion: $\text{minimize}_\Theta \sum_{(\boldsymbol{x},\boldsymbol{p},\boldsymbol{y}) \in \mathscr{T}_{\text{train}}} \|\boldsymbol{y} - r(\boldsymbol{x}, \boldsymbol{p}|\Theta)\|^2_{\Omega_{\boldsymbol{p}}}$, where $\Omega_{\boldsymbol{p}}$ stands for the brain region of interest, namely, that with meaningful E-field values. By considering a coil-centered coordinate system (see Supplementary Materials for details), the regression problem is simplified as

$$\underset{\Theta}{\text{minimize}} \sum_{(\tilde{\boldsymbol{x}},\tilde{\boldsymbol{y}}) \in \tilde{\mathscr{T}}_{\text{train}}} \|\tilde{\boldsymbol{y}} - r_0(\tilde{\boldsymbol{x}}|\Theta)\|^2_{\Omega_0}, \tag{1}$$

where $\tilde{\boldsymbol{x}}$, $\tilde{\boldsymbol{y}}$, and Ω_0 stand for the MR image, E-fields, and brain region of interest in a coil-centered coordinate system, respectively. A few examples of pairs of MR images $\tilde{\boldsymbol{x}}$ and E-fields $\tilde{\boldsymbol{y}}$ are shown in Fig. 4. Any regression model can be used for $r_0(\tilde{\boldsymbol{x}}|\Theta)$ in general, such as kernel-based regression [20,21], randomForest [22,23], and neural networks [24]. In this study, we employed a neural-network based regression model because of its high representation ability, well-established optimization algorithms, and computational efficiency. Fig. 5 shows a volume-to-volume neural network architecture named "U-Net" [17,25], which is used in our experiments. U-Net inputs a T1 MR image of size $(72 \times 144 \times 24)$ and outputs the absolute value of the induced E-field of the same size, namely, $(72 \times 144 \times 24)$. It consists of many 3D-convolution layers with batch normalization (BN) [26], rectified linear units (ReLU) [27], max pooling, and up-sampling. In addition, U-Net holds detailed local information using its skip connections.

More details of the physical model-based computation method and the DNNs are provided in Section 1 in the Supplementary Materials.

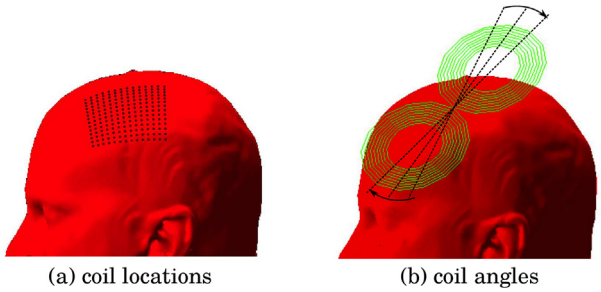

Fig. 3. Coil locations and angles. There are 7056 coil positions for all combinations of (14×14) locations and 36 angles.

Leave-five-cases-out validation

We validated the proposed estimation method of TMS-induced E-fields by training with 32 subjects and testing with 5 subjects. Thus, we had $32 \times 7056 = 225{,}792$ samples for training, and 5×7056 samples $= 35{,}280$ for testing (volume conductor computations). Three DNN models shown in Fig. 5 were used to demonstrate the difference of performance come from the difference of depth. For each model, we optimized the model parameter Θ for minimizing the cost function (1) by using the stochastic gradient descent (SGD) algorithm [28,29]. In the SGD algorithm, the parameter Θ is iteratively updated using backpropagation [30] for a mini-batch, which is a small subset containing a few (e.g., 5–50) training samples. We iteratively updated Θ for 20 epochs, where an epoch refers to a unit of iterations throughout the whole training set. Note that we did not use validation set for early stopping the optimization. After the optimization, DNN models with Θ were used for regression. The proposed DNN models were evaluated by comparing them with the VCM results for subjects that were not included in the training.

Results

Validations of the relative positions to the TMS coil

Focusing on the same voxel position of the estimated E-fields on the coil-centered coordinate for all $35,280$ testing samples, we calculated the correlation coefficient between the VCM and DNN model. Fig. 6 visualizes the values of those correlations for all

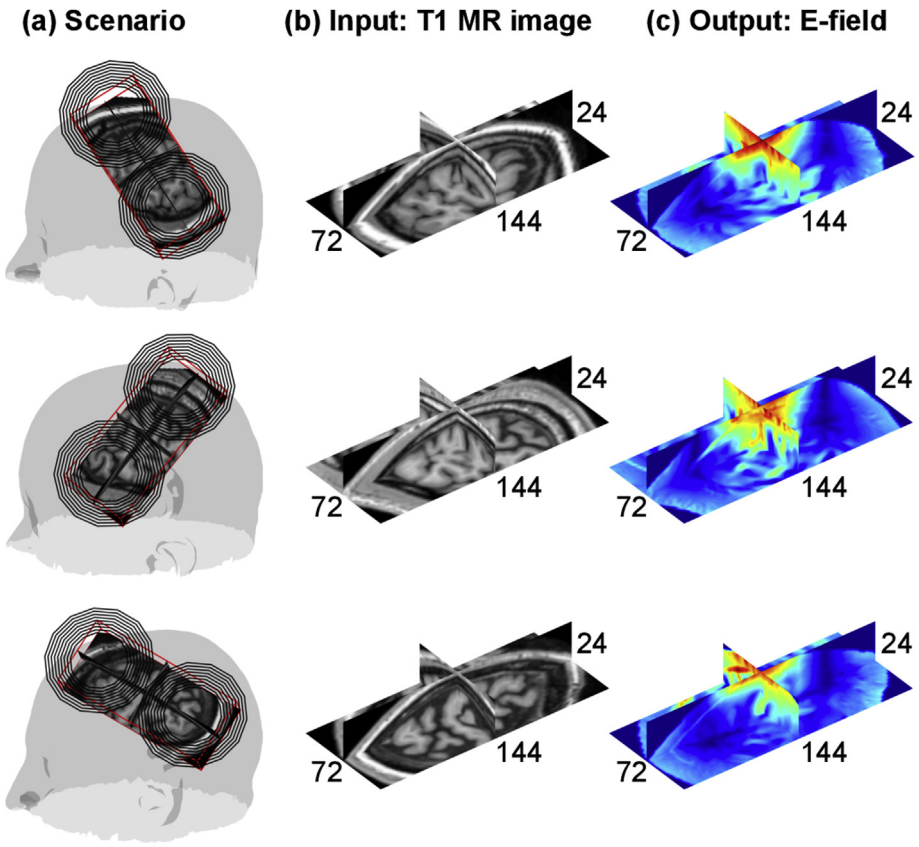

Fig. 4. Input/Output of the regression: our neural network model inputs a (72,144,24)-MR image and outputs a (72,144,24)-E-Field. Coil-centered T1 MR images (b), $\tilde{\boldsymbol{x}}$, are extracted from the original T1-MR image based on the corresponding coil positions, as shown in (a). Similarly, the corresponding E-fields for training (c), $\tilde{\boldsymbol{y}}$, are extracted from the original results by the VCM. Then, the DNN model automatically relates the inputs to its corresponding outputs.

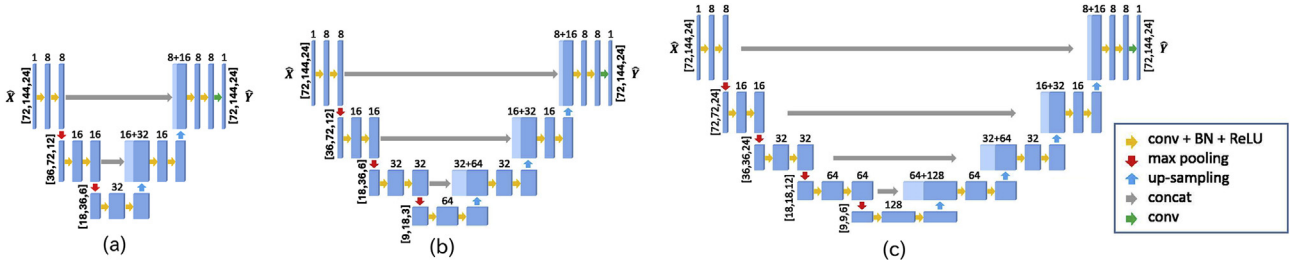

Fig. 5. Network architecture applied to the learning of TMS-induced electric field: Convolutional DNN model (named U-Net) with depths of (a) 2, (b) 3, and (c) 4.

voxel positions and the density plots of E-fields for some specific positions. The positions in white are located outside the head, and the correlations could not be calculated because of the zero variance of the E-fields. Almost all meaningful positions had positive correlations, and the higher values were obtained by deeper networks (see Supplementary Figs. 4 and 5). Notably, correlation coefficients on 95% of the meaningful relative positions of coil (*i.e.,* region excluding centers of coil wings and outside the brain) were higher than 0.8. The peripheral positions (e.g., (a) and (g) in Fig. 6) that bounce in and out of the head region had higher correlations since zero and non-zero values can be easily estimated. The centers of two coils wings (e.g., (b) and (f) in Fig. 6) have relatively low correlations because of the low strength of the E-fields. With the exception of those positions, the center and deeper positions (e.g., (c), (d), and (e) in Fig. 6) are highly accurate in general.

Target regions

The E-field distributions on the brain surfaces were compared by using the VCM computation and DNN estimations to confirm their usefulness for two target areas, a motor area (hand knob area) and a language area (Broca's area) which are considered important in presurgical diagnoses. Note that Broca's area is outside of training set, and here we report the interpolation performance by hand knob area and the extrapolation performance by Broca's area.

MR images of five subjects excluded from the training data were chosen, and the coil center was positioned so that it coincided with that of Broca's area or the hand knob area. The angle of the coil was fixed as 90° and 45° for Broca's area and the hand knob area, respectively. The angle of 45° for the hand knob area was based on clinical guidelines [31], while that for Broca's area was chosen arbitrarily as no guideline exists.

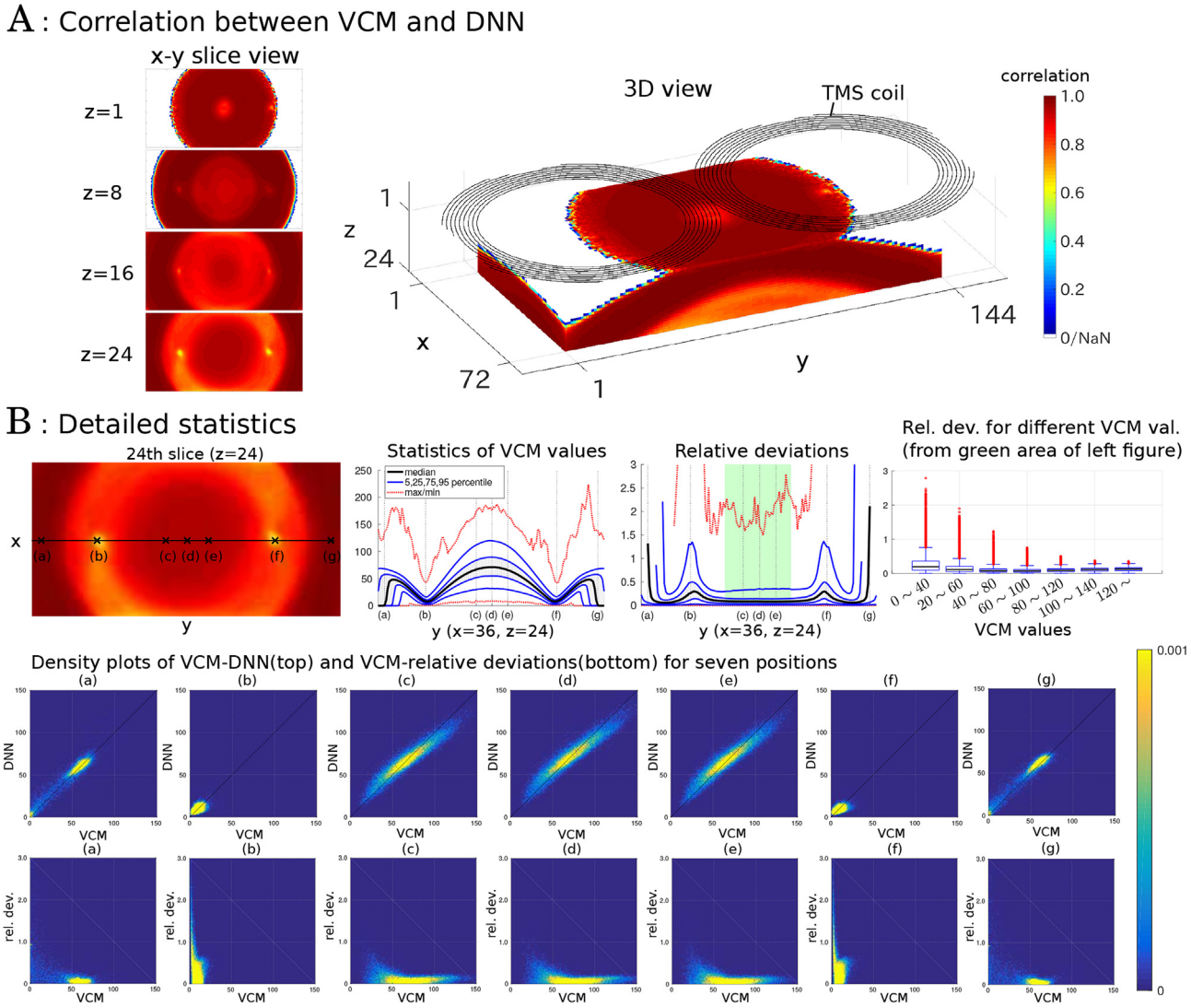

Fig. 6. Correlation analysis between E-fields estimated by the VCM and DNN model(depth 4): The top figure (A) shows the 3D heat maps of correlations between the VCM and DNN model in the coil-centered coordinate system. The correlation coefficient of each voxel is calculated with its corresponding voxel values of E-fields estimated by the VCM and DNN model for all 35,280 testing samples from the five subjects. The difference in the accuracy of the DNN model with respect to the relative positions to the TMS coil is shown. The bottom figure (B) shows the details of the statistics with density plots for several remarkable relative positions of the TMS coil. Different statistics can be observed for different positions. Furthermore, we summarized statistics of relative absolute deviations with boxplot for various E-field levels. The maximum relative deviations are shown from the highest markers in box plots. The accuracy of DNN was usually high for strong E-field levels.

Fig. 7 shows the results of estimated E-fields on the surfaces of gray matter extracted by FreeSurfer. The E-fields on the surface were computed by the linear interpolation of the voxel representations. The clear similarity between the VCM results and DNN estimations can be confirmed from the results. Specifically, the regions having higher values in the VCM and DNN almost overlapped (see the last columns in Fig. 7(A) and (B)). Table 1 shows the correlation coefficients,[3] peak signal-to-noise ratio (PSNR) [dB], mean absolute error (MAE) [V/m], and mean relative absolute deviations (RMAD) [%] between the two E-field surfaces of the VCM and DNNs for those two coil positions for the five subjects. For reference, we also calculated the E-fields using a homogenized volume conductor model (*i.e.,* all tissues of the head were assigned the conductivity of gray matter) and the primary E-field (*i.e.,* the time derivative of the magnetic vector potential). It is shown that the accuracy of DNN with depth 4 was much higher than the two references. Values of DNN approximately equal to 0.93 and 0.97 of the average correlation coefficients were obtained for Broca's area and the hand knob area, respectively. Roughly, PSNR was larger than 29 dB, MAE and RMAD were smaller than 6 V/m and 6% in hand knob area.

Comparing computation times

We compared the computation times for the VCM and individual DNN models. Table 2 shows the expected values of computation times for obtaining the output of one trial of an induced E-field from an MR image or human head model with one given coil position. The computation of the DNN was conducted by a single workstation with an Intel(R) Core(TM) i7-6850K CPU with a frequency of 3.60 GHz, 128 GB memory, and NVIDIA GeForce GTX 1080

[3] Since the surface is represented by many triangles of various shapes, we considered the *weighted correlation* based on the area of the triangles. Moreover, we ignored the area outside the head, which has meaningful values in DNN regression.

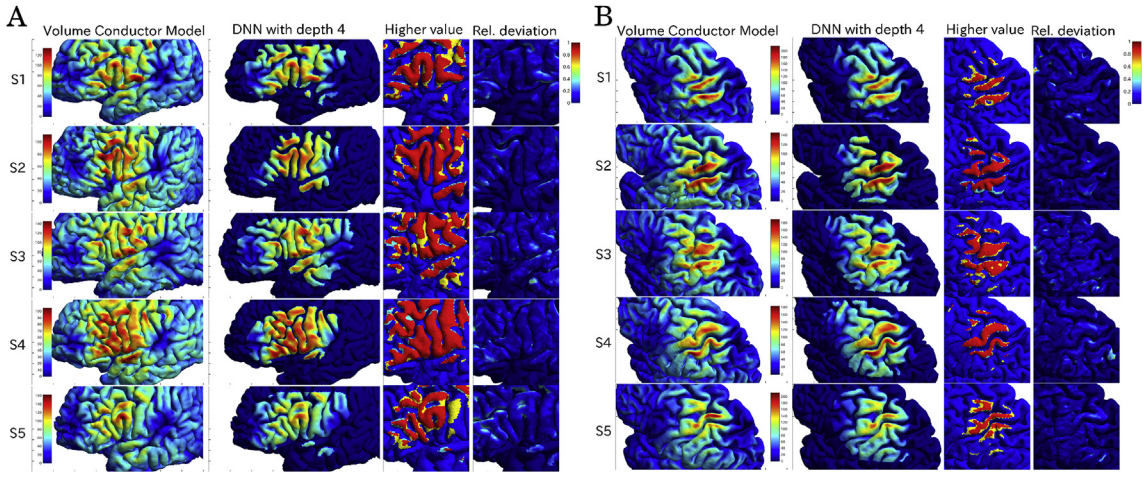

Fig. 7. Visual comparison of E-fields [V/m] obtained by the VCM and DNN model (depth 4) for the areas of interest: (A) Broca's area (outside the 14-by-14 grid) and (B) hand knob area (inside the 14-by-14-grid). The E-fields estimated by the DNN model are very similar to the volume conductor modeling results for five different subjects (S1–S5). Color maps of both the VCM and DNN model visualizations are equivalent in each subject. The second last column of both (A) and (B) shows the regions with electric field values higher than 50% of the maximum value in only the VCM (cyan) and only DNN model (yellow). The overlapped regions between the VCM and DNN model are depicted in red. The last column of both (A) and (B) shows the relative absolute deviation between VCM and DNN. (For interpretation of the references to colour in this figure legend, the reader is referred to the Web version of this article.)

Table 1
Correlation/PSNR[dB]/MAE[V/m]/RMAD[%] between the VCM and references/DNNs on brain surfaces.

Broca's area (outside the 14-by-14 grid)					
	homogenized model	primary E-fields	DNN(depth 2)	DNN(depth 3)	DNN(depth 4)
S1	0.741/22.5/11.88/11.95	0.707/14.4/35.88/50.79	0.865/24.7/9.73/10.07	0.933/27.0/7.25/6.51	0.938/27.2/6.89/6.12
S2	0.847/26.4/7.47/8.74	0.731/13.9/39.51/58.45	0.748/23.3/10.05/8.93	0.853/24.6/9.04/8.75	0.934/28.5/5.51/5.81
S3	0.858/24.4/9.51/10.27	0.790/15.7/30.86/41.71	0.796/22.7/11.69/11.64	0.897/24.7/9.41/8.60	0.932/26.3/7.60/6.77
S4	0.868/26.3/7.77/8.52	0.774/14.0/39.19/56.10	0.893/25.0/9.35/8.00	0.920/25.6/8.89/8.03	0.944/28.8/5.74/5.68
S5	0.853/24.3/9.93/10.65	0.780/14.3/36.74/51.13	0.818/23.4/10.98/10.87	0.910/24.6/9.23/8.27	0.927/25.4/8.31/7.44
ave.	0.833/24.8/9.31/10.02	0.757/14.5/36.44/51.64	0.824/23.8/10.36/9.90	0.903/25.3/8.76/8.03	0.935/27.2/6.81/6.37
std.	0.052/1.6/1.78/1.42	0.036/0.7/3.48/6.44	0.057/1.0/0.96/1.46	0.031/1.0/0.87/0.90	0.006/1.4/1.19/0.73
Hand knob area (inside the 14-by-14 grid)					
	homogenized model	primary E-fields	DNN(depth 2)	DNN(depth 3)	DNN(depth 4)
S1	0.695/17.8/19.17/18.44	0.706/14.0/36.94/53.17	0.953/26.2/7.83/7.30	0.977/29.1/5.33/4.87	0.984/30.5/4.61/4.20
S2	0.778/20.6/14.94/15.84	0.757/13.7/39.24/55.46	0.957/29.4/5.62/5.68	0.964/29.8/5.13/5.12	0.974/31.3/4.34/4.44
S3	0.810/20.1/15.23/15.40	0.793/15.3/31.81/44.36	0.946/26.2/8.09/7.62	0.974/28.3/6.18/5.93	0.979/29.6/5.34/5.20
S4	0.799/20.4/14.09/14.29	0.771/15.4/31.64/44.55	0.933/25.3/9.01/8.91	0.963/28.6/5.88/5.90	0.979/31.2/4.20/4.11
S5	0.729/19.8/14.87/15.59	0.690/14.4/35.54/50.40	0.936/26.3/7.27/6.80	0.969/28.9/5.27/4.94	0.977/30.1/4.41/4.30
ave.	0.762/19.7/15.66/15.91	0.744/14.6/35.03/49.59	0.945/26.7/7.56/7.26	0.969/28.9/5.56/5.35	0.979/30.6/4.58/4.45
std.	0.049/1.1/2.01/1.53	0.044/0.7/3.30/5.02	0.010/1.6/1.25/1.18	0.006/0.6/0.45/0.52	0.004/0.7/0.45/0.44

Table 2
Computation times.

models	computation time per trial
VCM (multi-grid)	3.034 [s]
DNN (depth 4, CPU)	0.541 [s]
DNN (depth 4, GPU)	0.024 [s]

Ti. Each value was calculated as the average time consumed for 10,000 trials in TensorFlow with/without GPU. One trial refers to an input of one MR image (i.e., the batch size is one) and an output of one E-field. For reference, the computation time of the VCM was measured with an Intel(R) Xeon(R) Gold 5120 CPU with a frequency of 2.20 GHz × 2 and 98 GB memory. Note that the computation time for the VCM does not include the lengthy construction process for an anatomical human head model which takes a few hours' or longer computation. This comparison confirms that the computation time of the DNN with GPU showed an extreme improvement over the conventional method.

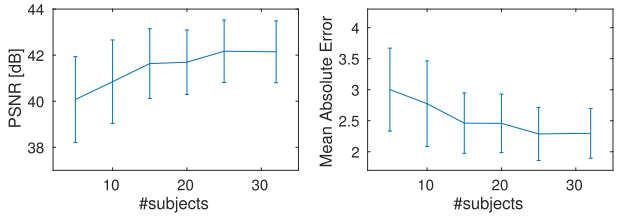

Fig. 8. Effects of number of subjects for training. The graph shows average and standard deviation of PSNR and MAE of all ($14 \times 14 \times 36 \times 5$) testing E-fields estimated by DNN trained with 5, 10, 15, 20, 25, and 32 subjects' MR brain images.

Number of subjects for training

We tried to change the numbers of subjects for training in $\{5, 10, 15, 20, 25, 32\}$, and evaluated the constructed DNNs with the same 5 testing subjects. Fig. 8 shows the average and standard deviations of PSNR and MAE for all DNNs. There is almost no difference when the number of subjects exceeds 15. It implies that the

variation of (72,144,24)-volumes in coil-centric coordinate would be captured by training with almost 15 subjects, and it supports our experiments using 32 subjects for training.

Discussion and conclusion

In this study, we first applied deep learning to relate E-fields computed by volume conductor modeling and medical images. It was shown that the field distribution can be estimated solely from T1 MR images, without the need for any physical computation. The effectiveness of the proposal was demonstrated by comparing the computed (i.e., by the VCM) and estimated E-fields for stimulating Broca's area and the hand motor area.

In conventional volume conductor modeling, the most time-consuming aspect concerns the segmentation and construction of subject-specific anatomical head models. In the proposed approach, segmentation is not required once the machine learning has been conducted. We confirmed that the image of the E-field is provided in 0.024 s accurately in the area of the maximum E-field. This is much quicker than a single computation of volume conductor computation using common software, as well as tissue segmentation from MR images.

There are commercially available neuronavigation systems that superpose an empirically estimated E-field on the medical images. However, this simple estimation does not model the distortion of the E-field due to individual brain anatomy. While the accuracy of the proposed DNN approach could still be improved, it can, nonetheless, capture the effect of anatomical features on the E-field distribution (Figs. 6 and 7, Table 1). The approach could thus provide more precise determination of stimulated brain areas compared to simple E-field models [9].

One motivation of this work was to provide the stimulation parameters (coil angle, injection current, and other such factors) for optimizing the E-field distribution on the brain in almost real time. The computation time to estimate the E-field was only 0.024 s for DNN with a depth of 4, using a conventional workstation with a GPU. This means simply that 40–50 coil positions can be simulated per second in real time during neuronavigation. The input data required for the DNN are the same as for conventional neuronavigation, namely, the T1 image and coil position. Therefore, the approach is very practical and could serve as an add-on for existing neuronavigation systems.

The approach does, however, suffer from some limitations. The first limitation is common for all VCMs. The proposed approach only allows a direct estimation of the E-field distribution, which is the physical agent of the stimulation, rather than the stimulation itself. Thus, the estimation is not directly associated with the electrostimulation [11]. The biophysical mechanism, including the relative angle of the E-field and axon [2,9,10,32,33], is not considered because the E-field is still widely used for estimating the target area. Another specific limitation of the machine learning approach is the uncertainty of the results obtained from the outlying inputs (e.g., pathological MR images with/without tumors). It might be avoided by augmenting the training dataset to contain various types of MR images; however, collecting a large number of real MR images is not easy and can be time-consuming. Synthetic data augmentation techniques will be helpful for improving the robustness of outliers although doing so is not a fundamental solution.

The DNN model constructed in this study is specific for one type of TMS coil. Since the induced E-field distribution differ with respect to the type of magnetic coil [34], a DNN model constructed using different coil models/TMS settings cannot be used for estimations by different condition. The differences in DNN models between different magnetic coils/TMS settings remains to be solved.

Some degradation of MR image quality or difference of the characteristics of MR images with respect to scanning devices/techniques would degrade the estimation of DNN. From a recent computer vision study [35], a benefit of convolutional neural network (CNN) structure that CNN itself has noise impedance has been discussed, and it would support the noise robustness of the proposed approach since U-Net is a CNN. Moreover, a simple solution of these issue is collecting various MR images scanned by various devices/techniques/situations. If it is difficult to collect a large number of MR images, a machine learning technique of "domain adaptation" [36] would be helpful to solve this issue, and it is included in future work.

The size of input/output MR/E-field volume was set as ($72\ \text{mm} \times 144\ \text{mm} \times 24\ \text{mm}$) in our experiments, and then limitation of deep surface was 24 mm, currently. However, the size of the volume can be easily changed, and extended toward more deep setting based on target applications.

The proposed DNN model outputs the magnitude of the induced E-field, which is useful for real-time navigated TMS. However, the model can be modified to output the vector components of the E-field with a marginal changes. A similar approach can be used for different applications, such as modeling transcranial direct current stimulation.

Author declaration

We wish to confirm that there are no known conflicts of interest associated with this publication and there has been no significant financial support for this work that could have influenced its outcome.

We confirm that the manuscript has been read and approved by all named authors and that there are no other persons who satisfied the criteria for authorship but are not listed. We further confirm that the order of authors listed in the manuscript has been approved by all of us.

We confirm that we have given due consideration to the protection of intellectual property associated with this work and that there are no impediments to publication, including the timing of publication, with respect to intellectual property. In so doing we confirm that we have followed the regulations of our institutions concerning intellectual property.

We further confirm that any aspect of the work covered in this manuscript that has involved either experimental animals or human patients has been conducted with the ethical approval of all relevant bodies and that such approvals are acknowledged within the manuscript.

We understand that the Corresponding Author is the sole contact for the Editorial process (including Editorial Manager and direct communications with the office). He/she is responsible for communicating with the other authors about progress, submissions of revisions and final approval of proofs. We confirm that we have provided a current, correct email address which is accessible by the Corresponding Author and which has been configured to accept email from t.yokota@nitech.ac.jp.

List of all authors:

- Tatsuya Yokota (corresponding author)
- Toyohiro Maki
- Tatsuya Nagata
- Takenobu Murakami
- Yoshikazu Ugawa
- Ilkka Laakso
- Akimasa Hirata
- Hidekata Hontani

Acknowledgments

This study was supported in part by a Japan Society for the Promotion of Science (JSPS) Grant-in-Aid for Scientific Research on Innovative Area (Multidisciplinary Computational Anatomy): JSPS KAKENHI Grant Number 26108003. The authors would like to thank Shinta Aonuma and Takashi Sakai for their quick and helpful assistance.

Appendix A. Supplementary data

Supplementary data to this article can be found online at https://doi.org/10.1016/j.brs.2019.06.015.

References

[1] Rossi S, Hallett M, Rossini PM, Pascual-Leone A, of TMS Consensus Group S, et al. Safety, ethical considerations, and application guidelines for the use of transcranial magnetic stimulation in clinical practice and research. Clin Neurophysiol 2009;120:2008–39.
[2] Bungert A, Antunes A, Espenhahn S, Thielscher A. Where does TMS stimulate the motor cortex? Combining electrophysiological measurements and realistic field estimates to reveal the affected cortex position. Cerebr Cortex 2016;27:5083–94.
[3] Thielscher A, Opitz A, Windhoff M. Impact of the gyral geometry on the electric field induced by transcranial magnetic stimulation. Neuroimage 2011;54:234–43.
[4] Opitz A, Windhoff M, Heidemann RM, Turner R, Thielscher A. How the brain tissue shapes the electric field induced by transcranial magnetic stimulation. Neuroimage 2011;58. 849–9.
[5] Opitz A, Legon W, Rowlands A, Bickel WK, Paulus W, Tyler WJ. Physiological observations validate finite element models for estimating subject-specific electric field distributions induced by transcranial magnetic stimulation of the human motor cortex. Neuroimage 2013;81:253–64.
[6] Windhoff M, Opitz A, Thielscher A. Electric field calculations in brain stimulation based on finite elements: an optimized processing pipeline for the generation and usage of accurate individual head models. Hum Brain Mapp 2013;34:923–35.
[7] Laakso I, Hirata A, Ugawa Y. Effects of coil orientation on the electric field induced by TMS over the hand motor area. Phys Med Biol 2014;59:203–18.
[8] Laakso I, Murakami T, Hirata A, Ugawa Y. Where and what TMS activates: experiments and modeling. Brain Stimulation: Basic, Translational, and Clinical Research in Neuromodulation 2018;11:166–74.
[9] Opitz N, Zafarb Alexander anad, Bockermannb V, Rohdeb V, Paulus W. Validating computationally predicted TMS stimulation areas using direct electrical stimulation in patients with brain tumors near precentral regions. Neuroimage: Clinic 2014;4:500–7.
[10] Aonuma S, Gomez-Tames J, Laakso I, Hirata A, Takakura T, Tamura M, Muragaki Y. A high-resolution computational localization method for transcranial magnetic stimulation mapping. Neuroimage 2018;4:85–93.
[11] Laakso I, Hirata A. Fast multigrid-based computation of the induced electric field for transcranial magnetic stimulation. Phys Med Biol 2012;57:7753–65.
[12] Makarov S, Noetscher G, Raij T, Nummenmaa A. A quasi-static boundary element approach with fast multipole acceleration for high-resolution bioelectromagnetic models. In: IEEE transactions on biomedical engineering; 2018.
[13] Dale AM, Fischl B, Sereno MI. Cortical surface-based analysis: I. segmentation and surface reconstruction. Neuroimage 1999;9:179–94.
[14] Fischl B, Sereno MI, Dale AM. Cortical surface-based analysis: Ii: inflation, flattening, and a surface-based coordinate system. Neuroimage 1999;9:195–207.
[15] Fischl B, Dale AM. Measuring the thickness of the human cerebral cortex from magnetic resonance images. Proc Natl Acad Sci Unit States Am 2000;97:11050–5.
[16] Goodfellow I, Bengio Y, Courville A, Bengio Y. Deep learning, vol. 1. MIT press Cambridge; 2016.
[17] Ronneberger O, Fischer P, Brox T, U-net. Convolutional networks for biomedical image segmentation. In: International conference on medical image computing and computer-assisted intervention (MICCAI). Springer; 2015. p. 234–41.
[19] Can MK, Laakso I, Nieminen JO, Murakami T, Ugawa Y. Coil model comparison for cerebellar transcranial magnetic stimulation. Biomedical Physics & Engineering Express 2019;5. 015020.
[20] Hastie T, Tibshirani R. Generalized additive models. Wiley Online Library; 1990.
[21] Drucker H, Burges CJ, Kaufman L, Smola AJ, Vapnik V. Support vector regression machines. In: Advances in neural information processing systems. NIPS; 1997. p. 155–61.
[22] Breiman L. Random forests. Mach Learn 2001;45:5–32.
[23] Liaw A, Wiener M, et al. Classification and regression by randomForest. R News 2002;2:18–22.
[24] Specht DF. A general regression neural network. IEEE Trans Neural Netw 1991;2:568–76.
[25] Çiçek Ö, Abdulkadir A, Lienkamp SS, Brox T, Ronneberger O. 3D U-net: learning dense volumetric segmentation from sparse annotation. In: International conference on medical image computing and computer-assisted intervention (MICCAI). Springer; 2016. p. 424–32.
[26] Ioffe S, Szegedy C. Batch normalization: accelerating deep network training by reducing internal covariate shift. In: International conference on machine learning; 2015. p. 448–56.
[27] Glorot X, Bordes A, Bengio Y. Deep sparse rectifier neural networks. In: Proceedings of the fourteenth international conference on artificial intelligence and statistics; 2011. p. 315–23.
[28] Duchi J, Hazan E, Singer Y. Adaptive subgradient methods for online learning and stochastic optimization. J Mach Learn Res 2011;12:2121–59.
[29] Kingma DP, Ba J. Adam: a method for stochastic optimization. 2014. 1412.6980.
[30] Rumelhart DE, Hinton GE, Williams RJ. Learning representations by back-propagating errors. Nature 1986;323:533–6.
[31] Rossini PM, Burke D, Chen R, Cohen L, Daskalakis Z, Di Iorio R, Di Lazzaro V, Ferreri F, Fitzgerald P, George M, et al. Non-invasive electrical and magnetic stimulation of the brain, spinal cord, roots and peripheral nerves: basic principles and procedures for routine clinical and research application. an updated report from an i.f.c.n. committee. Clin Neurophysiol 2016;126:1071–107.
[32] Laakso I, Murakami T, Hirata A, Ugawa Y. Experiments and modelling pinpoint the cortical activation site of TMS. Brain Stimulation: Basic, Translational, and Clinical Research in Neuromodulation 2017;10:460–1.
[33] Seo H, Jun SC. Relation between the electric field and activation of cortical neurons in transcranial electrical stimulation. Brain Stimulation; 2018.
[34] Deng Z-D, Lisanby SH, Peterchev AV. Electric field depth–focality tradeoff in transcranial magnetic stimulation: simulation comparison of 50 coil designs. Brain Stimulation 2013;6:1–13.
[35] Ulyanov D, Vedaldi A, Lempitsky V. Deep image prior. In: IEEE conference on computer vision and pattern recognition; 2018. p. 9446–54.
[36] Ganin Y, Ustinova E, Ajakan H, Germain P, Larochelle H, Laviolette F, Marchand M, Lempitsky V. Domain-adversarial training of neural networks. J Mach Learn Res 2016;17:1–35.